Analysis of the Photonic Band Gaps for Gyrotron devices

Yanyan Zhang, Sheng Yu, Liang Zhang, Tianzhong Zhang, Youwei Yang and Hongfu Li

***Abstract* — The global band gaps of the photonic crystal is theoretical analyzed in this paper. The electromagnetic wave propagation characteristics of the photonic band gap (PBG) structures, which are interested in the millimeter wave, sub-millimeter wave, and terahertz regime vacuum electronic devices and accelerators, were numerically simulated by using the finite-element method software HFSS. The dispersion curves of the lattices in different ratios of the rod radius to the rod spacing, and the global band gaps for the general two-dimensional PBG structures formed by triangular and square arrays of metal rods were simulated. A mode map which shows the relationship between the structures and the contained modes was plotted and a 220 GHz metallic PBG resonator operates at TE_{04} mode was designed for a gyrotron device to verify the theoretical and numerical simulations, and the comparison of the mode density and the quality factor between the PBG resonator and the equivalent cylindrical resonator have been analyzed.**

***Index Terms* —PBG, gyro-devices, square lattice, triangular lattice, cavity resonator**

I. Introduction

Vacuum electron devices are important high power microwave radiation sources for their applications in industrial heating, plasma diagnostics, radar, communications, driving accelerators and so on [1-4]. Increasing the operating frequency is of great interest and will promote new applications in more areas. One way to achieve higher frequency is to scale down the interaction structure dimensions, however it also limits the power handling of the waveguide structures as well as increases the machining difficulty. The other way to increasing the operating frequency as well as keeping high power capability is to operate at higher order modes. However, it usually suffers from the mode competitions from the neighbor modes [4, 5]. To obtain high interaction efficiency, single-mode excitation is desired and the RF circuit needs to be selective with respect to the operating mode, and the undesired oscillations should be suppressed. The use of photonic band gap (PBG) structures, especially 2D PBG structures, have been experimentally proved to be a promising approach for the realization of mode selective circuits by introducing point or line defect in the photonic crystal (PC) array by using the trapping property of the PBG structure.

In recent years, numerous advances in the theoretical and numerical simulations allow better understanding of the PBG structures [6]. This led to new applications in passive devices for guiding and confining the electromagnetic radiation [3-12]. A PBG cavity operating at a TE_{041}-like mode produced a peak power of 25 kW at 140 GHz has been demonstrated at MIT. No competing modes were observed over a 30% minimum frequency bandwidth of the design mode [4]. Another gyrotron amplifier based on the PBG interaction cavity achieved a peak small signal gain of 38 dB and 45 W output power at 247.7 GHz has also been developed in MIT. The experiment achieved the highest operation frequency for a gyrotron amplifier. And it is the first amplifier that is capable of producing either high gain or high output power at such high frequency range [3].

The design of the PGB structures requires an accurate prediction of the global photonic band gaps, which is still challenging and time consuming. Several methods to analyze the PBG structure have been proposed and in-house-built codes have been developed, such as the modified plane wave expansion (PWE) method [15], the transfer matrix method (TMM) [16, 17] and the finite-difference time-domain method (FDTD) [18], and the coordinate-space finite-difference method (CSFD) [7]. In this paper, the simulation method using the commercial finite element method electromagnetic solver to calculate the band gap characteristics of photonic crystals is introduced. The simulation results agree well with the published data. The proposed method allows to study more complicate PBG structures without the need to develop own codes, which will save great effort.

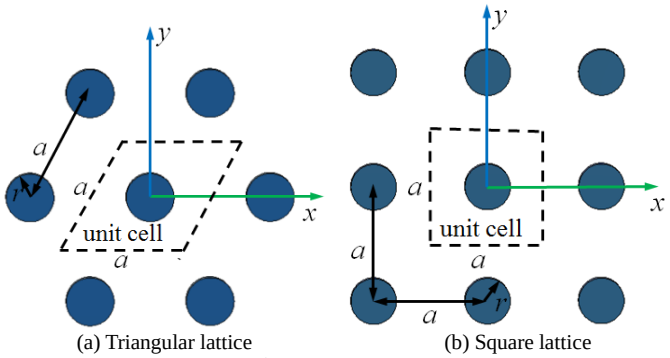

(a) Triangular lattice (b) Square lattice

Fig. 1. Cross-section view of the 2D PBG structures with metal cylinders in a triangular (a) and square (b) lattice. The fundamental unit cells are within the dash lines.

Y. Zhang, S. Yu, T. Zhang, Y. Yang, H. Li are with the Terahertz Science and Technology Research Center, School of Physical Electronics, Department of Physics, University of Electronic Science and Technology of China, Chengdu 610054 China. (e-mail: zhangyan.ueste@gmail.com).

Y. Zhang, L. Zhang are with Department of Physics, SUPA, University of Strathclyde, Glasgow G4 0NG UK. (e-mail: liang.zhang@strath.ac.uk).

II. Theory of PBG Structures

In this paper, two types of metal lattices are considered, including the triangular lattices and the square lattice, shown as Fig. 1.

These structures can be fully described by the periodic conductivity profile, which satisfies the periodic condition

$$\sigma(\vec{x}_\perp + \vec{T}_{mn}) = \sigma(\vec{x}_\perp) \tag{1}$$

where the periodicity vectors $\vec{T}_{mn}$ are defined as

$$\vec{T}_{mn} = \begin{cases} (m+n/2)a\vec{e}_x + \sqrt{3}/2\, na\vec{e}_y \ (\text{triangular lattice}) \\ ma\vec{e}_x + na\vec{e}_y \ (\text{square lattice}) \end{cases} \tag{2}$$

where a is the lattice spacing, m and n are integers and $\vec{x}_\perp = x\vec{e}_x + y\vec{e}_y$.

Since the system is homogeneous along the Z direction, the Helmholtz wave equation for $\psi(\vec{x}_\perp)$ derived from the Maxwell's equations becomes

$$\nabla_\perp^2 \psi(\vec{x}_\perp) = \left(k_z^2 - \omega^2/c^2\right)\psi(\vec{x}_\perp) \tag{3}$$

The boundary conditions for the TE and TM modes on the surfaces of the metallic rods, which is denoted by S, are

$$\left.\frac{\partial \psi}{\partial \vec{n}}\right|_s = 0 \quad \text{(TE mode)} \tag{4}$$

$$\psi|_S = 0 \quad \text{(TM mode)} \tag{5}$$

where $\vec{n}$ is the normal vector to the rod surface.

Due to the discrete translational symmetry of the conductivity profile, the fundamental solution of the Helmholtz equation can be written as the Bloch's form

$$\psi(\vec{x}_\perp + \vec{T}_{mn}) = \psi(\vec{x}_\perp)e^{i\vec{k}_\perp \cdot \vec{T}_{mn}} \tag{6}$$

where $\vec{k}_\perp = k_x\vec{e}_x + k_y\vec{e}_y$ is the vector of the transverse wave number. Therefore only the electromagnetic field inside the fundamental unit cell needs to be solved. From Fig. 1, the boundaries of the fundamental unit cell are given by

$$\left|x - y/\sqrt{3}\right| \le a/2, \left|y\right| \le \sqrt{3}a/4 \ \text{(Triangular lattice)} \tag{7}$$

$$\left|x\right| \le a/2, \left|y\right| \le a/2 \qquad \text{(Square lattice)} \tag{8}$$

and the periodic boundary conditions are given by:

Triangular lattice:

$$\begin{cases} \psi\left(a/2 + y/\sqrt{3}, y\right) = e^{ik_x a}\psi\left(-a/2 + y/\sqrt{3}, y\right) \\ \psi\left(x, \sqrt{3}a/4\right) = e^{ik_x a/2 + ik_y\sqrt{3}a/2}\psi\left(x - a/2, -\sqrt{3}a/4\right) \end{cases} \tag{9}$$

Square lattice:

$$\begin{cases} \psi\left(-a/2, y\right) = e^{ik_x a}\psi\left(a/2, y\right) \\ \psi\left(x, -a/2\right) = e^{ik_y a}\psi\left(x, a/2\right) \end{cases} \tag{10}$$

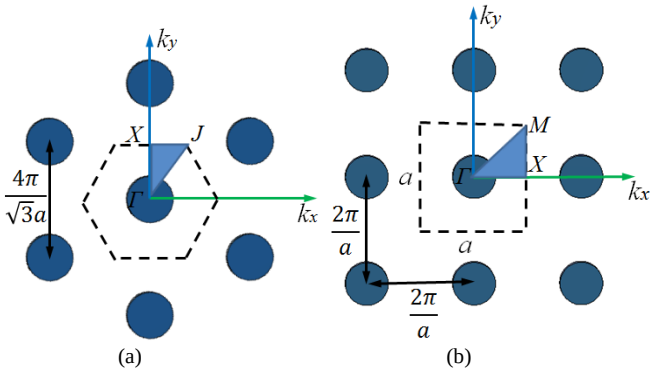

Fig. 2. Reciprocal lattices and Brillouin zones for triangular (a) and square (b) lattice PBG structures. The irreducible Brillouin zones are shown shaded.

The periodicity of the exponent in (6) restricts the possible values of $\vec{k}_\perp$ to the irreducible Brillouin zones of the reciprocal lattices [10], the Brillouin zones for both cases of triangular and square lattices are shown in Fig. 2. The three special points Γ, *X*, *J* for triangular lattice and special points Γ, *X*, *M* for square lattice are

$$\left.\begin{aligned} &\Gamma : \vec{k}_\perp = 0 \\ &X : \vec{k}_\perp = \frac{2\pi}{\sqrt{3}a}\vec{e}_y \\ &J : \vec{k}_\perp = \frac{2\pi}{\sqrt{3}a}\left(\frac{1}{\sqrt{3}}\vec{e}_x + \vec{e}_y\right) \end{aligned}\right\} \text{(Triangular lattice)} \tag{11}$$

$$\left.\begin{aligned} &\Gamma : \vec{k}_\perp = 0 \\ &X : \vec{k}_\perp = \frac{\pi}{a}\vec{e}_x \\ &M : \vec{k}_\perp = \frac{\pi}{a}\left(\vec{e}_x + \vec{e}_y\right) \end{aligned}\right\} \qquad \text{(Square lattice)} \tag{12}$$

With these special points the phase of the Helmholtz wave at each point can be decided from (11) and (12). Then using phase scan for Brillouin zones can complete the exploration of the propagation characteristics of electromagnetic waves through a PBG structure which will be introduced in section III.

III. Simulations of the Global Band Gaps for the 2D PBG Structures

The wave equation with the periodic boundaries can be numerically solved. In this paper, the commercial finite element method solver high frequency structural simulator (HFSS) was used. As only the TE modes are interested for gyro-devices, the perfect magnetic boundary can be defined on the top and bottom of the unit cell to make sure only the TE modes are solved. The periodic boundary conditions were achieved by using the master and slave boundaries, as shown in Fig. 3, which defines the phase advance across the two orthogonal directions of the unit cell.

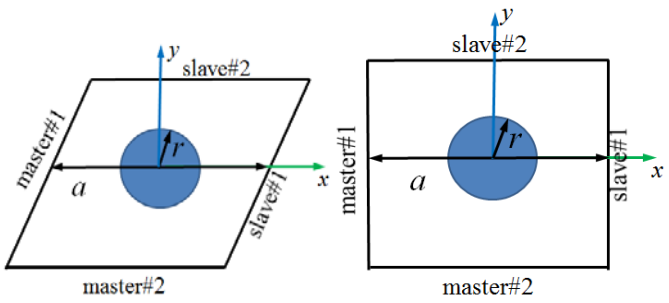

(a) Triangular lattice (b) square lattice

Fig. 3. Master/slave boundaries for triangular and square lattice unit cell

The wave numbers at *x*, *y* directions were then calculated by (9) and (10) for triangular and square lattice respectively. For example, going from the Γ point to the *X* point of Fig. 2 (a), k_x will always be zero, but k_y will be in the range of $[0, 2\pi/(\sqrt{3}a)]$. In this case, the first equation in (9) indicates a phase shift $\phi_1 = 0$ from the master #1 to the slave #1 boundary and the other equation in (9) indicates a phase shift between 0 and π from the master #2 to the slave #2 boundaries in Fig. 3(a). Performing the same analysis from *X* to *J* and *J* to Γ will complete the exploration of the Brillouin zones can be studied using parameter scans in the closed lines by points Γ, *X* and *J*. The same approach can be used to analyze the square lattice. The parameter ranges of k_x and k_y and the corresponding phase shifts of the master/slave boundaries for triangular and square lattice are listed in table I and table II, respectively.

TABLE I

THE SIMULATION PARAMETERS TO INVESTIGATE THE BRILLOUIN ZONE FOR THE TRIANGULAR LATTICE

	k_x	k_y	ϕ_1	ϕ_2
Γ to *X*	0	$0 \to 2\pi/\sqrt{3}a$	0	$0 \to \pi$
X to *J*	$0 \to 2\pi/3a$	$2\pi/\sqrt{3}a$	$0 \to 2\pi/3$	$\pi \to 4\pi/3$
J to Γ	$2\pi/3a \to 0$	$2\pi/\sqrt{3}a \to 0$	$2\pi/3 \to 0$	$4\pi/3 \to 0$

TABLE II

THE SIMULATION PARAMETERS TO INVESTIGATE THE BRILLOUIN ZONE FOR THE SQUARE LATTICE

	k_x	k_y	ϕ_1	ϕ_2
Γ to *X*	$0 \to \pi/a$	0	$0 \to \pi$	0
X to *M*	π/a	$0 \to \pi/a$	π	$0 \to \pi$
M to Γ	$\pi/a \to 0$	$\pi/a \to 0$	$\pi \to 0$	$\pi \to 0$

Figs. 4 and 5 show the simulated dispersion characteristics for the TE modes at different rod-to-lattice ratios *r/a* equal to 0.25 and 0.42, respectively. Only the first 10 lowest modes of the normalized frequencies as a function of $k_\perp$ which varies from the center of Brillouin zone (point Γ) to the near edge (point *X*) and then to the far edge (point *J* for the triangular lattice and point *M* for the square lattice) are plotted. The most interesting propagation characteristics of the lattice lie in the regions of a global band gap where no modes are able to prorogated. From Fig. 4, where the rod-to-lattice ratio *r/a* is 0.25, a global band gap exists between the third and the fourth modes for the triangular lattice, while no global band gaps existing at the first 10 lowest modes for the square lattice. In Fig. 5, when increasing the values of *r/a*, for the triangular lattice a global band gap exists between the second and third mode, and other higher order global band gaps; for the square lattice, there is a global band gap between the first and second modes, and another higher order global band gaps as well. If the operating mode is designed to be trapped in the band gap by introducing defect while the undesired modes are in other places, the mode competition can be eliminated.

The plots on the global band gaps as a function of ratio of rods radii *r* to the rods spacing *a* would be helpful for understanding the PBG structure. Fig. 6 shows the global band gaps for the TE modes in triangular and square lattices. It agrees well with the results in ref. [7] which uses real-space finite difference method. The frequencies of the global band gaps for the TE modes are dependent on the *r/a* values in triangular and square lattices. Therefore given an operating frequency, it is possible to design a PBG resonator or a waveguide that has the mode selective characteristic from the characteristics of the photonic crystal obtaining in this section.

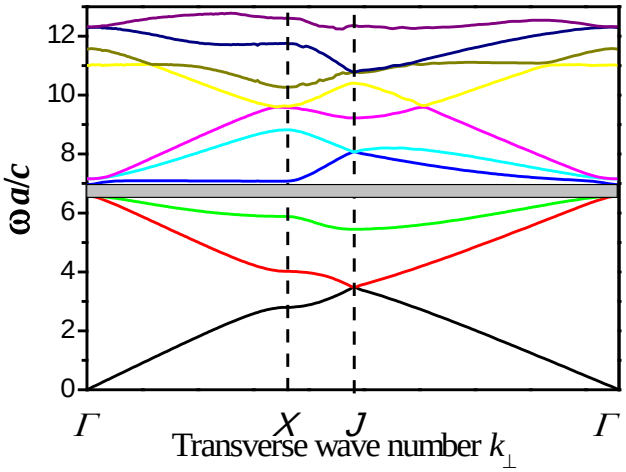

(a) Triangular lattice

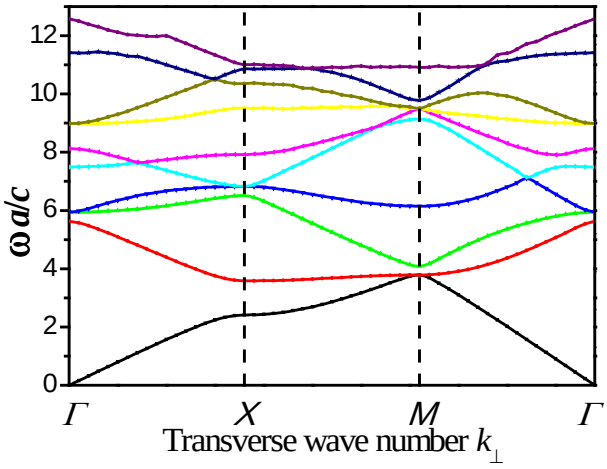

(b) Square lattice

Fig. 4. Normalized eigenmode frequencies as a function of $k_\perp$ for the (a) triangular lattice and (b) square lattice when $r = 0.25a$.

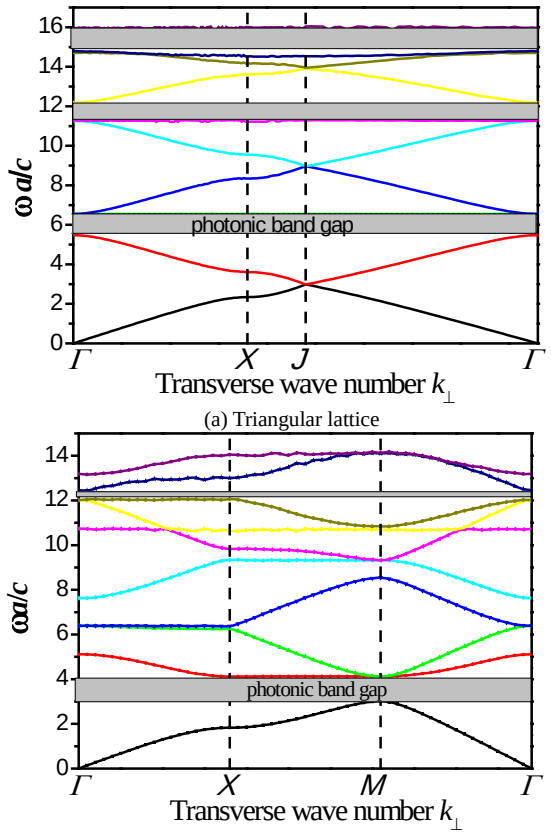

(a) Triangular lattice

(b) Square lattice

Fig. 5. Normalized eigenmode frequencies as a function of $k_\perp^{'}$ for the (a) triangular lattice and (b) square lattice when $r = 0.42a$.

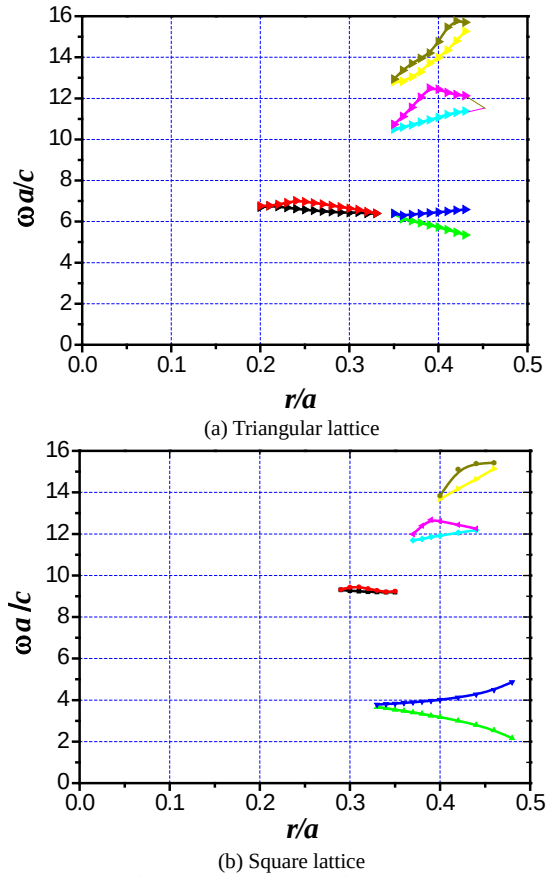

(a) Triangular lattice

(b) Square lattice

Fig. 6. The plot of the global band gap for (a) triangular lattice and (b) square lattice as a function of *r*/*a* values.

IV. Design for the PBG Interaction Circuit

The beam-wave interaction region in a Gyrotron requires high mode purity to achieve a high interaction efficiency, which can be achieved by using PBG structures as the interaction region. A PBG cavity can be formed by removing a certain amount of the metallic rods in the center. The possibility of the mode competition can be greatly reduced if the desired operating mode in the cavity falls within the forbidden band, and the other undesired modes fall within the pass band.

In a circular waveguide, the cut-off radius at a given frequency is

$$R = cx_{m,n}^{'} / (2\pi f) \tag{13}$$

where $x_{m,n}^{'}$ is the n^{th} zero roots of the m^{th}-order Bessel function $J_m^{'}(x)$. By matching the cutoff frequencies between the circular waveguide and the PBG structure, it is able to estimate the equivalent radius after removing some metallic rods. From Fig. 7, the equivalent interaction radius is $R = \sqrt{7}a - r$ and $R = \sqrt{3}a - r$ for removing 19 and 7 rods, respectively. Therefore we have

$$\lambda/a = \begin{cases} 2\pi/x_{mn}^{'}\left(\sqrt{7} - r/a\right) \\ 2\pi/x_{mn}^{'}\left(\sqrt{3} - r/a\right) \end{cases} \tag{14}$$

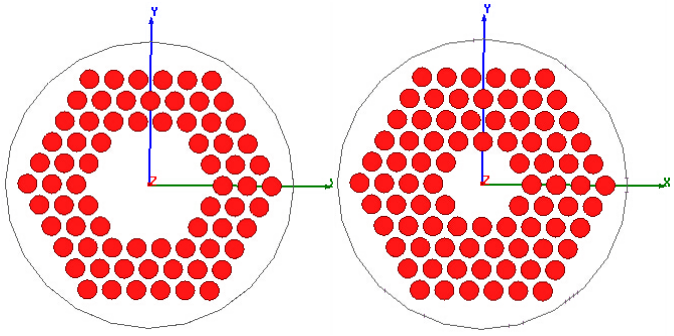

(a) (b)

Fig. 7. 2D triangular lattice metal rods with a central defect by removing (a) 19 and (b) 7 rods

According to (14) and the triangular lattice global band gap, a mode map which can be examine the occurrence of the possible modes in the PBG cavity with the relationship between *r*/*a* and λ/a can be obtained, shown in Figs. 8 and 9, where $\lambda = c/f$ is the wavelength of the mode $TE_{m,n}$ contained in the PBG cavity. And these figures can be used as the guidance of choosing the dimensions of the lattice and the operation mode.

When designing a gyrotron device, the operating frequency is usually known. Then the potential mode competitions of the possible operating mode can be examined from the Fig. 8 and 9. Once the operating mode is decided, the lattice vector a can be determined from the desired operating frequency and the shape of the lattice; and further decide the value of the rod radius. At the same time, as the operating frequency is depending on the *r*/*a* ratio, it is possible to change the radius of the rods to tune the operating frequency of the device.

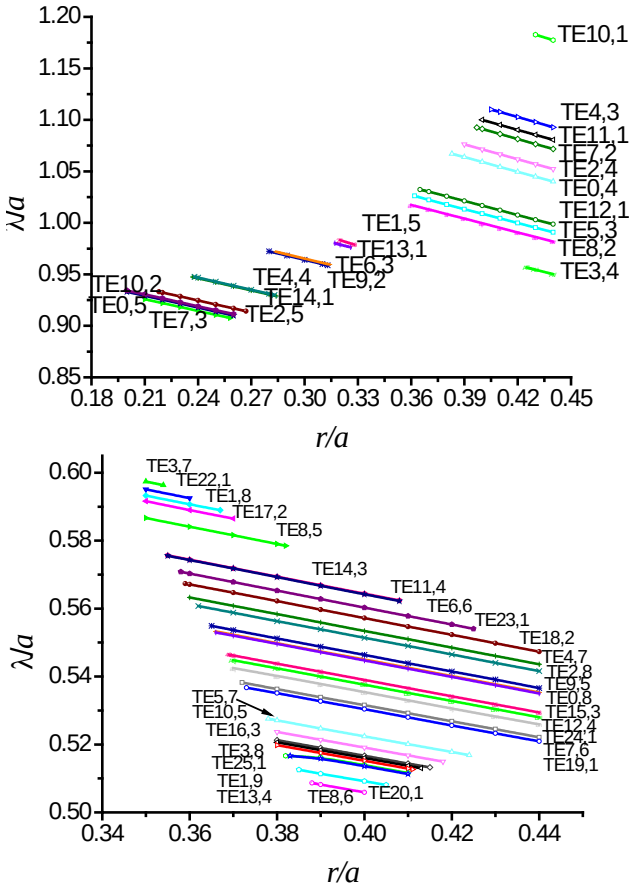

Fig. 8. The relationship between r/a and λ/a for different modes after removing 19 rods.

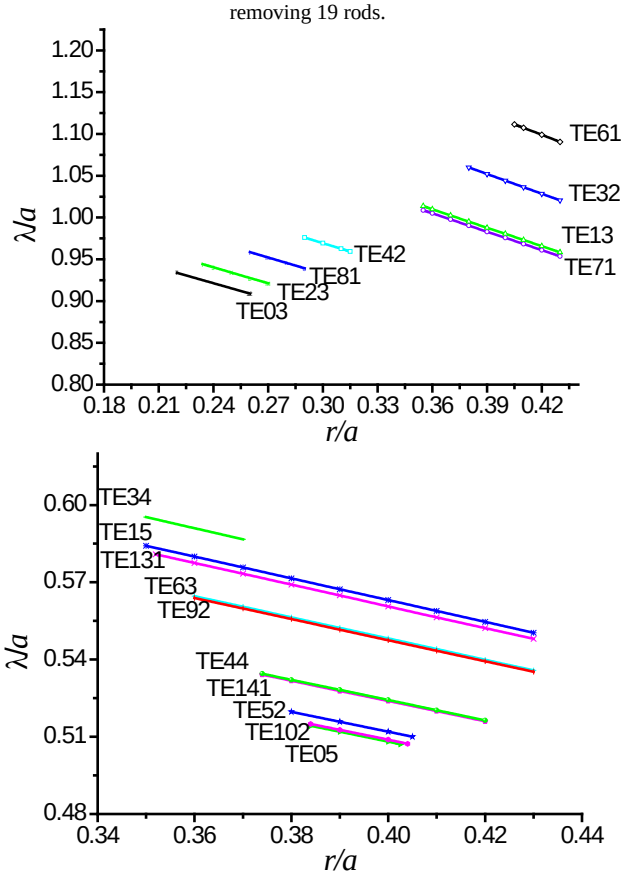

Fig. 9. The relationship between r/a and λ/a for different modes after removing 7 rods

A 220 GHz Gyrotron was designed and the eigen field was simulated. Compare with the equivalent radii of the PBG cavity, the one after removing 19 rods has larger diameter than the one after removing 7 rods. Therefore it was chosen as due to the higher power capability. The operating mode is TE_{04} as it has less mode competition and is able to get a better interaction with the electron beam. According to Fig. 8, the TE_{04} mode work in the range of $0.38<r/a<0.44$ and the normalized wavelength range is $1.0402<\lambda/a<1.06709$. The final parameters were chosen as a=1.29 mm, $\omega a/c$=5.9478 and r/a=0.39. The triangular lattice was chosen. The designed PBG gyrotron cavity was then verified by HFSS and the mode pattern of TE_{04} is shown in Fig. 10 (a). The empty circles denote the location of the rods since no electric field can exist at those locations. The frequency of the confined eignmode is 220.236 GHz in the TE_{04} mode, which agrees well with the result from the analytical calculation. From (14), the equivalent interaction radius can be calculated as $R=\sqrt{7}a-r=2.9$ mm for this PBG resonator. Fig. 10(b) shows the mode pattern of TE_{04} at the equivalent interaction radius of the cylindrical resonator. The mode pattern and the resonate frequency of the cylindrical resonator confirm that the method of equivalent cylindrical waveguide is correct to design the PBG resonator. Also to show the advantage of the PBG resonator that is able to alleviate the mode competition, table III shows the mode density in the PBG resonator compared with an equivalent cylindrical resonator. Only those modes without longitudinal variation (TE_{mn0}) are listed in table III because of the astronomical computation time and RAM requirements if all the modes are considered in such a large-size overmoded resonator.

TABLE III
COMPARISON OF THE MODE DENSITY IN THE PBG GYROTRON RESONATOR TO AN EQUIVALENT CYLINDRICAL RESONATOR.

Cyl. res. mode	Frequency (GHz)	Ohmic Q	PBG res. mode	Frequency (GHz)	Q
$TE_{4,3,0}$	211.052	16858.3			
$TE_{11,1,0}$	213.457	5307.41			
$TE_{7,2,0}$	215.571	14156.1			
$TE_{2,4,0}$	219.35	19268.9			
$TE_{0,4,0}$	221.935	19931.1	$TE_{0,4,0}$	220.236	10627.7
$TE_{12,1,0}$	231.277	5302.93			
$TE_{5,3,0}$	233.328	17850.5			
$TE_{8,2,0}$	233.454	14072.2			

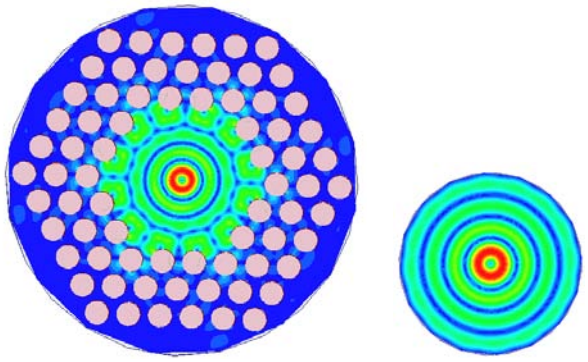

(a) (b)

Fig. 10. (a) The mode pattern of TE_{04}-like eigen mode in the PBG resonator at 220.236 GHz. (b) The mode pattern of TE_{04} eigen mode in the equivalent cylindrical resonator.

V. Conclusion

In this paper, the boundary conditions and the possible *k*-space of the photonic crystal fundamental unit cells are derived from the theoretical analysis. The band gaps of the photonic crystal with triangular lattice and square lattice are calculated using the commercial software HFSS by solving the boundary conditions. The dispersion curves as a function of the ratio of rods radius r to the rods spacing a, were also derived for the global band gaps for general two-dimensional PBG structures formed by triangular and square arrays of metal rods. The global band gap in the simulations agrees well with the results calculated by real-space finite difference method. A mode map has been also plotted to examine the occurrence of the possible modes in the PBG cavity. And a PBG cavity whose operating mode is TE_{04} at 220 GHz was designed based on the analytical and numerical results derived in this paper. The mode density and the quality factor of the designed PBG cavity was compared with the equivalent cylindrical resonator at the neighborhood modes around the operating frequency. The results demonstrate that the PBG resonator have more preponderance at suppression of the competing mode.

Acknowledgment

This paper is supported by China Scholarship Council under Program for Graduate Student Overseas Study Scholarship 2013 to 2014, hosted by Relativistic Electron and Laser Discharge (RELD) group, Department of Physics at the University of Strathclyde UK.

References

[1] W. He, C. R. Donaldson, L. Zhang, K. Ronald, P. McElhinney, and A. W. Cross, "High power wideband gyrotron backward wave oscillator operationg towards the terahertz region," *Phys. Rev. Lett.*, vol. 110, 165101, Apr. 2013.

[2] K. Felch, B. G. Danly, H. R. Jory, K. E. Kreishcher,W. Lawson, B. Levush, and R. J. Temkin, "Characteristics and Applications of Fast-Wave Gyro-devices," *Proc. Of the IEEE*, vol. 87, no. 5, pp. 752-781, May 1999.

[3] E. A. Nanni, S. M. Lewis, M. A. Shapiro, R. G. Griffin, and R. J. Temkin, "Photonic-band-gap traveling-wave gyrotron amplifier," *Phys. Rev. Lett.*, vol. 111, 235101, Dec. 2013

[4] J. R. Sirigiri., K. E. Kreischer, J. Macuhzak, I. Mastovsky, M. A. Shapiro, and R. J. Temkin. "A Photonic Band Gap Resonator Gyrotron," *Phys. Rev. Lett.*, vol. 86, no. 24, pp. 5628-5631, Jun. 2001

[5] J. R. Sirigiri, "A Novel Wideband Gyrotron Traveling Wave Amplifier. Massachusetts institute of technology," Ph.D. dissertations, Dept. Elect. Eng. Computer Sci., MIT, Cambridge, MA, USA, 2003.

[6] J. D. Joannopoulos, S. G. Johnson, J. N. Winn and R. D. Meade, "Photonic Crystals: Molding the Flow of Light," 2nd ed. Princeton Univ. Press, Princeton, NJ, 2007.

[7] E. I. Smirnova, C. Chen, M. A. Shapiro, J. R. Sirigiri, and R. J. Temkin, "Simulation of Photonic Band Gaps in Metal Rod Lattices for Microwave Applications," *J. App. Phys.*, vol. 91, no. 3, pp. 960-968, 2002.

[8] E. A. Nanni, "Design of a 250 GHz gyrotron amplifier," Ph.D. dissertation, Dept. Elect. Eng. Computer Sci., MIT, Cambridge, MA, USA, 2010.

[9] M. A. Shapiro, W. J. Brown, I. Mastovsky, J. R. Sirigiri, and R. J.Temkin, "17 GHz photonic bandgap cavity with improved input coupling," *Phys. Rev., Special Topics: Accelerators and Beams*, vol. 4, pp. 042001(1)–042001(6), 2001.

[10] E. I. Smirnova, M. A. Shapiro, C. Chen, and R. J. Temkin, "Photonic band gap structures for accelerator applications," in *AIP Con. Proc.*, Stony Brook, New York, USA, pp. 309-319, Jun. 2004.

[11] E. I. Smirnova, A. S. Kesar, I. Mastovsky, M. A. Shapiro, and R. J. Temkin, "Demonstration of a 17 GHz, high-gradient accelerator with a photonic-band-gap structure," *Phys. Rev. Lett.*, vol. 95, no. 7, pp. 074801.1-074801.4, 2005.

[12] E. I. Smirnova, C. Chen, and R. J. Temkin, "Theoretical analysis of overmoded dielectric photonic band gap structures for accelerator applications," in *Proc. of the 2003 Particle Accelerator Conf.*, pp. 1255-1257, Oregon, Portland, U.S.A., May 2003.

[13] L. Qi, Z. Yang, Z. Liang, W. Liu, Y. Liu, and X. Gao. "Design of Photonic Crystal Resonant Cavity Using Overmoded Dielectric Photonic Band Gap Structures," *Piers Online*, vol. 3, no. 4, pp. 379-381, 2007.

[14] T. Sakaguchi, O. Sakai, and K. Tachibana. "Photonic bands in two-dimensional microplasma arrays. II. Band gaps observed in millimeter and subterahertz ranges," *J. App. Phys.*, vol. 101, no. 7, pp. 073305.1-073305.7, 2007

[15] V. Kuzimiak, A. A. Maradudin, and F. Pincemin. "Photonic band structures of two-dimensional systems containing metallic components," *Phys. Rev. B*, vol. 50, no. 23, pp. 16835–16844, 1994.

[16] J. B. Pendry and A. Mackinnon, "Calculation of photon dispersion relations," *Phys. Rev. Lett.*, vol. 69, no. 19, pp. 2772–2775, Nov.9, 1992.

[17] M. Sigalas, C. M. Soukoulis, and E. N. Economou, "Photonic band gaps and defects in two dimensions: Studies of the transmission coefficient," *Phys. Rev. B*, vol. 48, no. 19, pp. 14121–14126, Nov. 1993.

[18] M. Qiu and S. He, "A nonorthogonal finite-difference time-domain method for computing the band structure of a two-dimensional photonic crystal with dielectric and metallic inclusions," *J. App. Phys.*, vol.87, no. 12, pp. 8268–8275, Jun. 2000.

Yanyan Zhang received the B.S. degrees in vacuum electronics from the University of Electronic Science and Technology of China (UESTC), Chengdu, China, in 2009 and be honored as outstanding graduate of UESTC. She is currently pursuing the Ph.D. degree in Physical electronics at UESTC. From 2013 to 2014, she was a visiting researcher with the Department of Physics, University of Strathclyde, UK. Her research interest is the Terahertz band Gyrotron including MIG gun, beam-wave interaction, microwave windows and so on.

Sheng Yu received the M.S. and Ph.D. degree in physical electronics from the University of Electronics Science and Technology of China (UESTC), Chengdu, China, in 1996 and 2002, respectively. He is a professor with UESTC and his current research interests include high power microwave devices.

Liang Zhang received the M.Sc. degree in application of nuclear techniques from the China Academy of Engineering Physics, Chengdu, China, in 2007, and the Ph.D. degree in physics from the University of Strathclyde, Glasgow, UK in 2012. He is currently a Research Associate with Department of Physics, University of Strathclyde. His main research interests include Gyrotron-TWA/backward-wave oscillators.